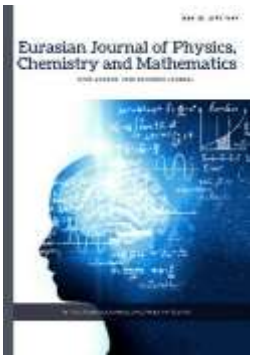

The effect of nickel on the sensitivity of plasmonic photonic crystal fiber sensor

Hussein Taqi John[1] — [1,2,] College of Science / Department of Physics / University of Wasit /Iraq/Wasit
* hjohn@uowasit.edu.iq

Imad Kamil Zayer[2] — [1,2,] College of Science / Department of Physics / University of Wasit /Iraq/Wasit

Ali Abed Jaber[3] — [3,] College of Education / Department of Physics / University of Wasit /Iraq/Wasit

ABSTRACT

In this work, a plasmonic optical fiber sensor is designed to sense liquid materials depending on the imaginary part of the effective refractive index responsible for the loss of these materials.

This sensor consists of two groups of circles, the first group contains six holes filled for air, and the second group outer is alternately filled with the analyte and air, and this arrangement is covered with a layer of a noble metal, which is nickel, to increase the efficiency of the sensor as it produces surface plasmon resonance (SPR), The proposed sensor was also surrounded by a layer (PML)to prohibit reflections in the middle of the sensor. The druid-Lorentz model was used to calculate the electrical permittivity of metals, and the Sellemier model was used to calculate the permittivity of silica.

The refractive indices of the analyzed material were chosen ($n_a = 1.37,\ 1.38,\ 1.39,\ 1.4$). The results of confinement loss and wavelength sensitivity showed that the first peaks appearing are when ($n_a = 1.37$), and the highest peaks and the best spacing are in the case of ($n_a = 1.4$). Where the best case obtained for the confinement loss, resonance wavelength, and wavelength sensitivity are in the case of nickel layer thickness ($d = 140\ nm$), radius of air holes ($R_1 = 0.40\ \mu m$), the radius of analyte holes ($R_2 = 1.9\ \mu m$), and radius of core ($r_1 = 2.4\ \mu m$).

Keywords: PCF, Nobel Metals, propagation constant, plasmonic fiber

1- Introduction

At the end of the last century's nineties, photonic crystal fibers (PCF) appeared for use in some optical applications, as these fibers differ according to their composition. There are three main types of these fibers, depending on the core type: solid core, hollow core, and porous core. Due to its composition's complexity and unique advantages, this fiber can be used in many applications, one of which is its use as a sensor. Researchers have designed hundreds of models to maximize the sensor's sensitivity by adding noble elements or some crystalline compounds to form the PCF [1].

$PCFs$ Have high cross-section design flexibility, and these fibers have attracted great interest from researchers due to their unique properties in refraction, dispersion, and

nonlinearity and their excellent performance in applications for fiber laser sensors and nonlinear optics [2]. PCF The cladding consists of many air holes embedded within the silica material background [3]. This is a breakthrough in optical fiber technology with conventional optical fibers, composed of one material with many engineering parameters that can be changed to achieve greater design flexibility [4].

PCF It is a fiber that is made of silica and contains microscopic holes. The guidance properties of the fibers are determined by parameters related to the air holes. With the variety of new or improved features of PCF fibers, their use is increasing in science and technology, unlike traditional fibers [5].

The property of plasmons and surface waves is generated through noble metals. The noble metal exhibits optical conductivity from the visible to the infrared region frequency because of interband transmission. Its high surface for volume proportion and optical plasmonic properties make it a proper filter for use as a sensor. Graphite or noble metals have sensor advantages based on increased particle absorption. Also, the electronic density of the hexagonal graphene rings prevents small atoms from passing through the ring structure, where the advantages of using graphene or noble metals are the SPR-based sensors [6].

SPR It is a collective vibration caused by the conjugation of electromagnetic waves and free electrons. This interaction binds to the interface between the metal and the insulator and leads to important field boost phenomena, thus SPW being especially sensitive to dielectric properties near the metal surface. In turn, changing RI at the interface modulates the highly concentrated electromagnetic fields generated by the SPR. This appearance leads to a direct wherewithal of monitoring surface events that can induce dielectric changes for plasmonic applications. Figure (1) represents plasmonic-based on SPP [7].

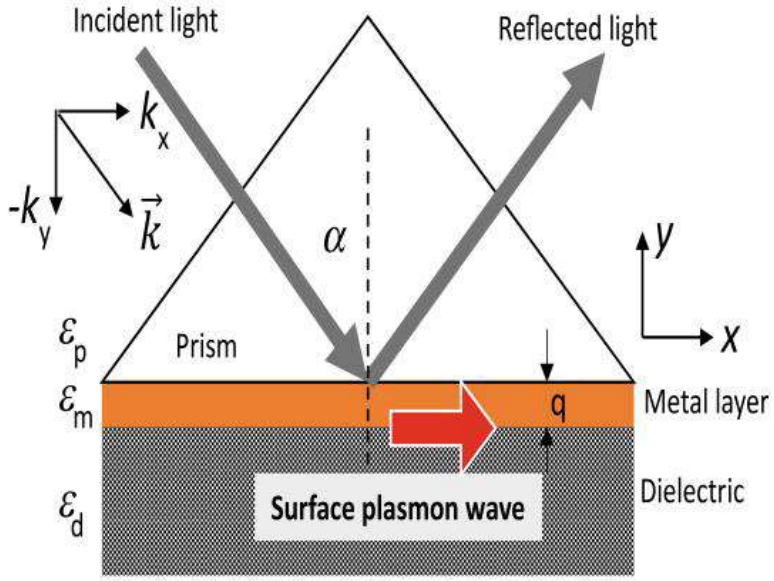

Fig.(1): Plasmonic PCF based on the SPP [8].

2
- design of the sensor

Figure (1) shows a diagram of the proposed sensor. This sensor consists of two groups of holes. The first group, the inner one, contains six small circular holes of radius R_1. It is filled with air, and the dimension between the center of any circle and the sensor's center is r_1. The dimension between the centers of any adjacent holes is Λ_1, while the second group, the outer one, contains eight circular holes. Of

these eight holes, four of which are half-large holes in diameter, R_2, filled with the analyte n_a, the dimension between the center of any of them and the center of the sensor r_2, the second four are small. The radius is R_1, filled with air, and the dimension between the centers of any adjacent holes (a large round hole and a small round hole) is Λ_2. This arrangement is covered with a layer of noble metal, nickel, with a thickness of d, and the distance between this layer and the center of the sensor is r_3. This sensor also has a layer called PML a layer, which is meant to absorb the scattered light. Table (1) contains the value of the parameter for this sensor.

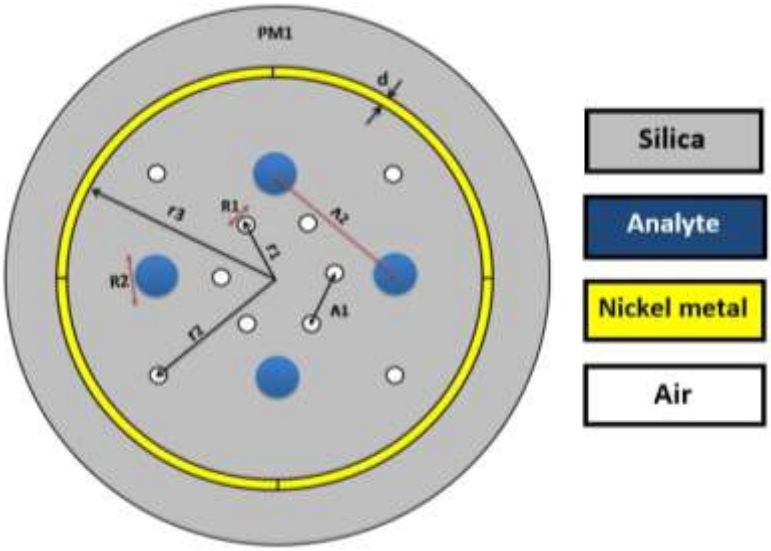

Fig.(2): Proposed sensor installation design

Table (1): parameters of proposed sensor installation design.

parameter	Simulation values	parameter	Tested values
r_1	2.3, 2.4 μm	h	9, 9.5 μm
Λ_1	0.6 r_1	R_1	0.39, 0.40 μm
r_2	0.6 h	R_2	1.8, 1.9 μm
Λ_2	0.7 h	d	140, 160 nm
r_3	8, 8.5 μm	n_a	1.37, 1.38, 1.39, 1.40 μm

3- paper concepts

The PCF sensor is mainly made from silica. Therefore, RI Selmer's equation can calculate the silica material [9].

$$n_{sil}^2(\lambda) = 1 + \frac{A_1\lambda^2}{\lambda^2 - B_1} + \frac{A_2\lambda^2}{\lambda^2 - B_2} + \frac{A_3\lambda^2}{\lambda^2 - B_3} \qquad (1)$$

Where n_{sil} is the RI silica, λ is the wavelength, and A_1, A_2, A_3 B_1, B_2, B_3 are constants for the coefficient of Sellmeier and taken from the source [10].

The electrical permittivity can be calculated according to the Drude-Lorentz model in the following form [11]

$$\varepsilon_r(w) = 1 - \frac{w_p^2}{w^2 + i\bar{\gamma} w} + \sum_i \frac{f_i w_i^2}{w_i^2 - w^2 - i\bar{\gamma}_i w} \qquad (2)$$

Where (w_i) is the resonance of frequencies, (i) represents the resonant modes, ($\bar{\gamma}_i$) represents the impact damping, and (f_i) refers to the weighting parameter. The ideal parameters for nickel metal for the Drude – Lorentz model are shown in Table (2).

Table (2): The ideal parameters of the Drude-Lorentz model [12].

Parameters	Ni
f_o	0.096
γ_d	0.048
f_1	0.100
$\gamma_1\ (eV)$	4.511
$\omega_1\ (eV)$	0.174
f_2	0.135
γ_2	1.334
ω_2	0.582
f_3	0.106
γ_3	2.178
ω_3	1.597
f_4	0.729
γ_4	6.292
ω_4	6.089
f_5	——
τ_5	——
ω_5	——

Optical mode leakage from the core of the optical fiber results in confinement loss. The air holes in the casing region are arranged so that the RI contrast is appropriately maintained so that the visual field remains in the core region. Insufficient RI contrast causes the light to travel away from the core into the envelope region, thus increasing the confinement loss. Hence, effective casing design with appropriate air-hole pitch and air-hole will help reduce confinement loss [13]. The loss of confinement (Lc) can be calculated from the imaginary part of the effective modal index as [14]

$$Lc\left(dB/cm\right) \approx 8.686 k_o Im\left\{n_{eff}\right\} \times 10^7 \qquad (3)$$

Where $Im\left\{n_{eff}\right\}$ is the imaginary part from the effective refractive index, and $k_o = 2\pi/\lambda$ is the wavenumber and the free-space wave vector. The wavelength sensitivity can be calculated as follows [15]

$$S(\lambda) = \frac{\partial \lambda_{peak}}{\partial n_a} \quad \left(\frac{nm}{RIU}\right) \qquad (4)$$

4. Results and Discussion

The COMSOL environment represents the relationship between (λ) and the effective refractive index. This program works on the finite element method ( ), which divides the medium into tiny parts and forms a mesh.

4.1 Nickel Metal Thickness

Figure (3) shows the relationship between the Lc (λ) of the different ($n_a = 1.37,\ 1.38,\ 1.39,\ 1.40$) using different thicknesses of the nickel metal ($d = 140,\ 160\ nm$). Where it was observed from Figure (1) that the highest and best divergence of the resonance peaks were obtained, It was observed when ($d = 140\ nm$) we obtained the highest amount of peaks and the first peak that appeared for ($n_a = 1.37,\ 1.38,\ 1.39,\ 1.40\ \mu m$), respectively.

As noted, when increasing (d), the peaks will shift to the left. This proposed sensor's results and sensitivity differ from designer to designer [16, 17, 18]. Table (3) shows the best wavelength sensitivity achieved at ($d = 140\ nm$) and decreases with increasing values of (d).

Table (1): wavelength sensitivity for metal thickness Ni .

$d\ (nm)$	Wavelength sensitivity (nm/RIU) for Ni
140	2500, 2000, 2500
160	2000, 2500, 2000

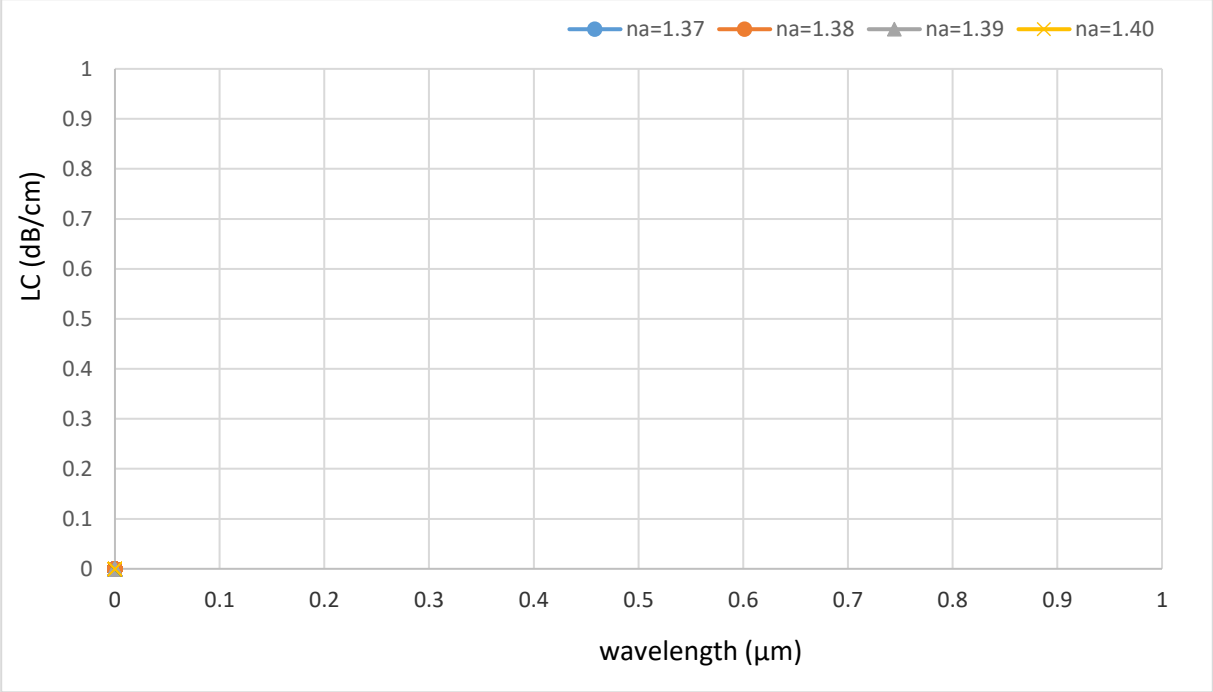

a

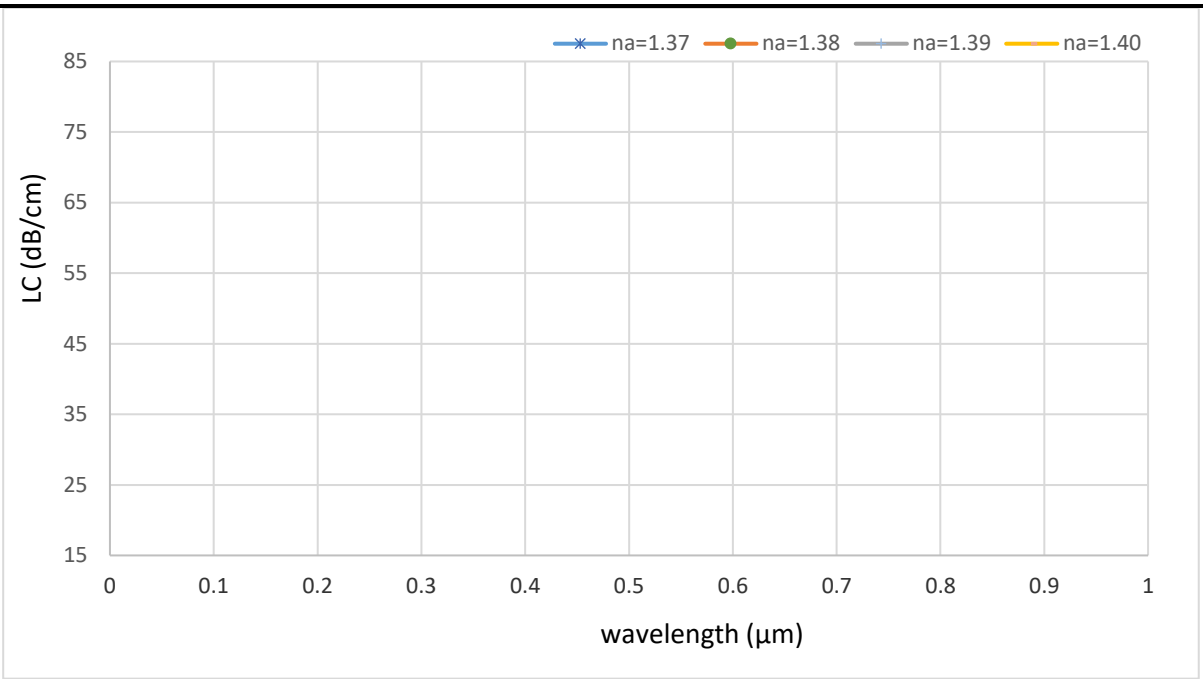

b

Figure (3): Represents the transient loss of nickel at ($n_a = 1.37,\ 1.38, 1.39, 1.40$), Where (a) represents ($d = 140\ nm$) and (b) represents ($d = 160\ nm$).

Figure (4) represents the relationship between the wavelength of resonance with the (n_a) for the thickness of nickel metal (d). It is noted from the figure that the resonance wavelength in both cases is approximately linear and can be passable to realized ideal design, as the linear relationship is what realizes the best sensor as long as the range can be developed to other values.

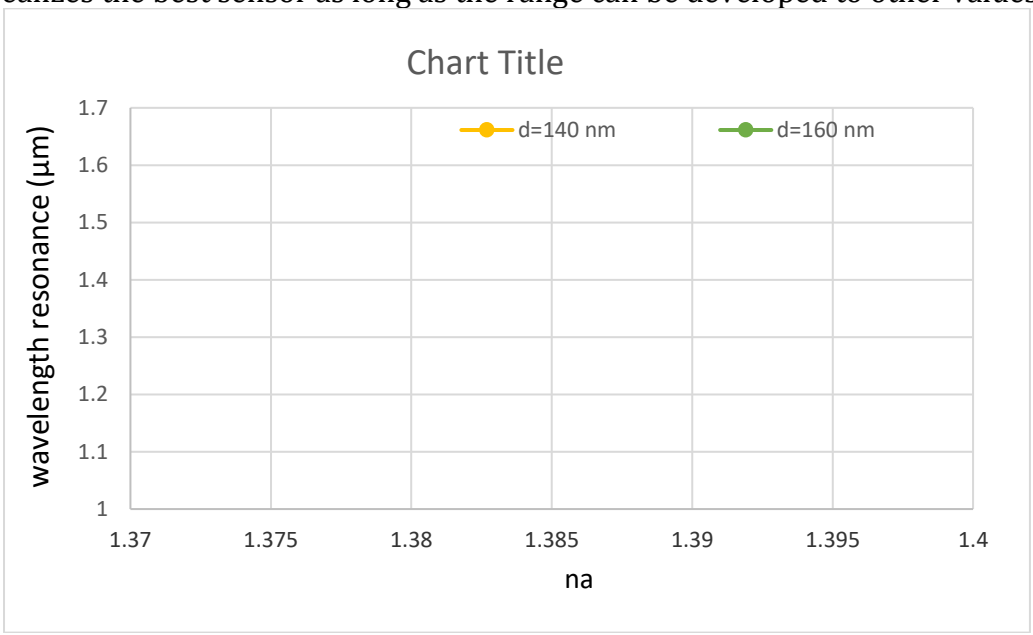

Figure (4): Resonance wavelength with the (n_a) when ($d = 140,\ 160\ nm$).

4.2 Effects of Air Holes Radius (R1)

Figure 5: represents the relationship between the Lc as a function of λ when the ($n_a = 1.37,\ 1.38, 1.39, 1.40$) and the radius of the air holes is ($R_1 = 0.39, 0.40\ \mu m$). The figure indicates that all the values of (R_1) realize distinct values and a good divergence between the peaks, and this spacing increases with the increased values (R_1). As it was observed, when increasing the amount of (n_a), the height of the peaks will increase, also when increasing the values of (R_1), the curves will creep to the right

Table (4): indicates the best wavelength sensitivity values at ($R_1 = 0.40\ \mu m$).

Table(4): wavelength sensitivity for different radii R_1 .

$R_1(\mu m)$	Wavelength sensitivity (nm/RIU)
0.39	1500, 2000, 1500
0.40	2500, 1500, 2000

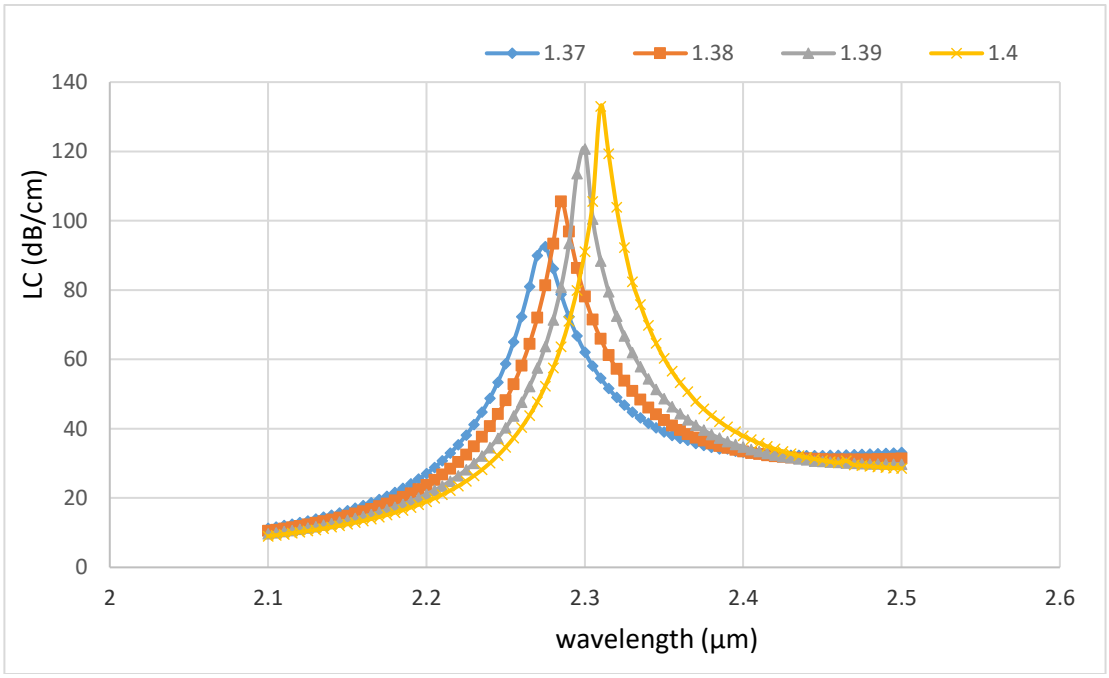

a

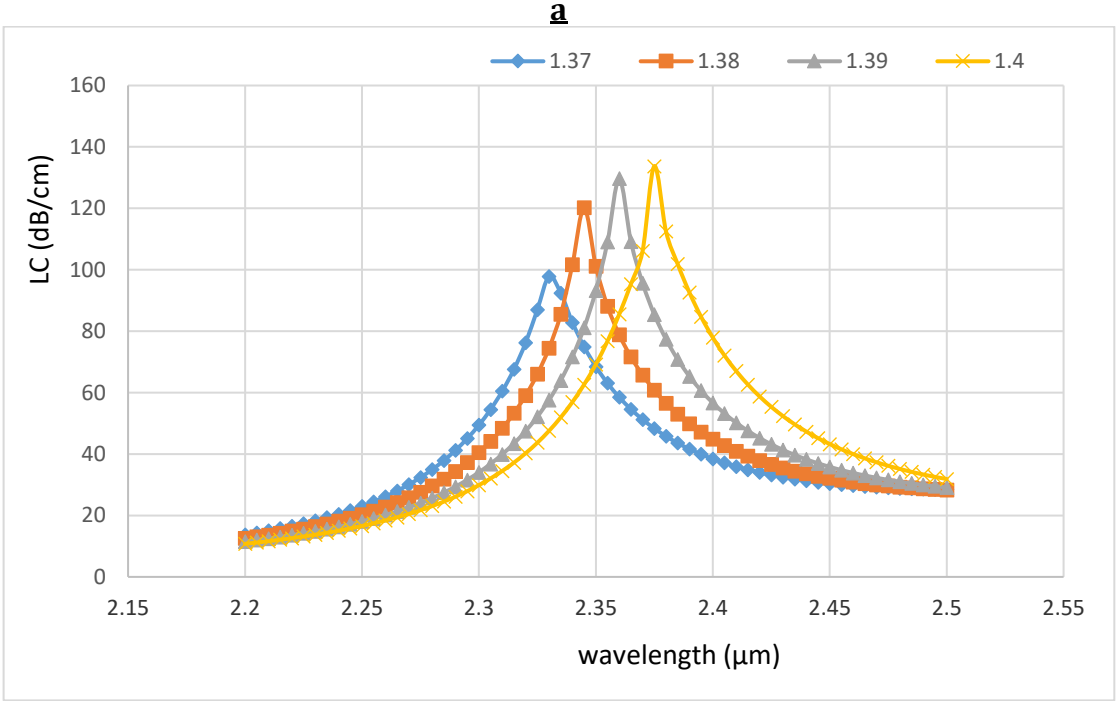

b

Figure (5): represents the confinement loss of nickel metal with λ when ($n_a = 1.37,\ 1.38,\ 1.39,\ 1.40$), Where (a) represents ($R_1 = 0.39\ \mu m$) and (b) represents ($R_1 = 0.40\ \mu m$)

Figure 6: represents the relationship between the resonance wavelength with (n_a) when ($R_1 = 0.39,\ 0.40$). From the figure, the relationships are almost linear, as the approaching linear relationship achieves the best sensor as long as the range (n_a) can be expanded to other values. We observe when the ($R_1 = 0.40\ \mu m$) relationship is very approaching linear and can be passable to fulfill the ideal design.

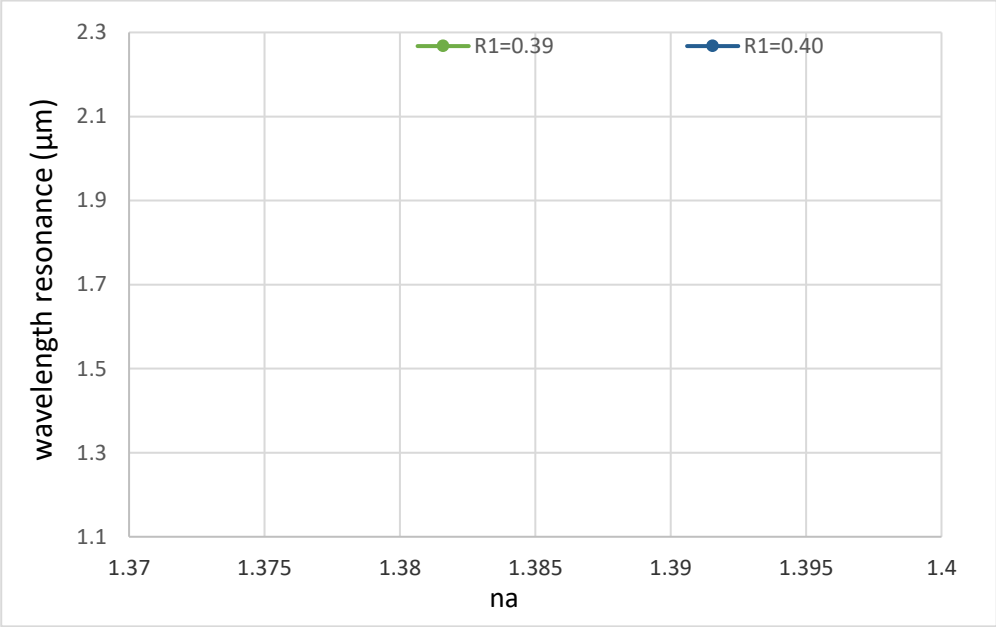

Figure (6): Resonance wavelength as a function of ($n_a = 1.37,\ 1.38, 1.39, 1.40$) when ($R_1 = 0.39,\ 0.40\ nm$).

4.3 Effects of Analyte Holes Radius (R2)

Figure (7): represents the relationship between Lc the λ refractive index of the ($n_a = 1.37,\ 1.38, 1.39, 1.40$) when the analyte holes radius ($R_2 = 1.8,\ 1.9\ \mu m$). It is noted from the figure that the highest and best divergence between the peaks is in the case of ($R_2 = 1.9\ \mu m$), and this case will be the best in terms of wavelength sensitivity and amplitude. Table (5) indicates the best wavelength sensitivity values at ($R_2 = 1.9\ \mu m$).

Table(5): wavelength sensitivity for different radii R_2 .

$R_2(\mu m)$	Wavelength sensitivity (nm/RIU)
1.8	1500, 2000, 2000
1.9	2000, 2500, 2000

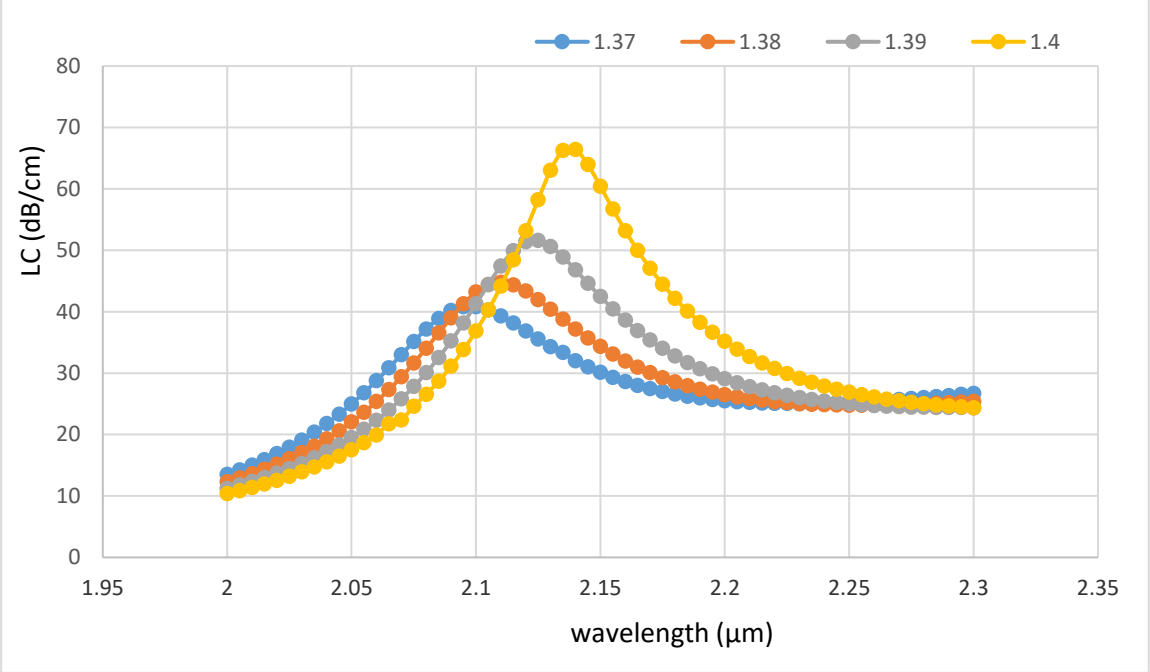

a

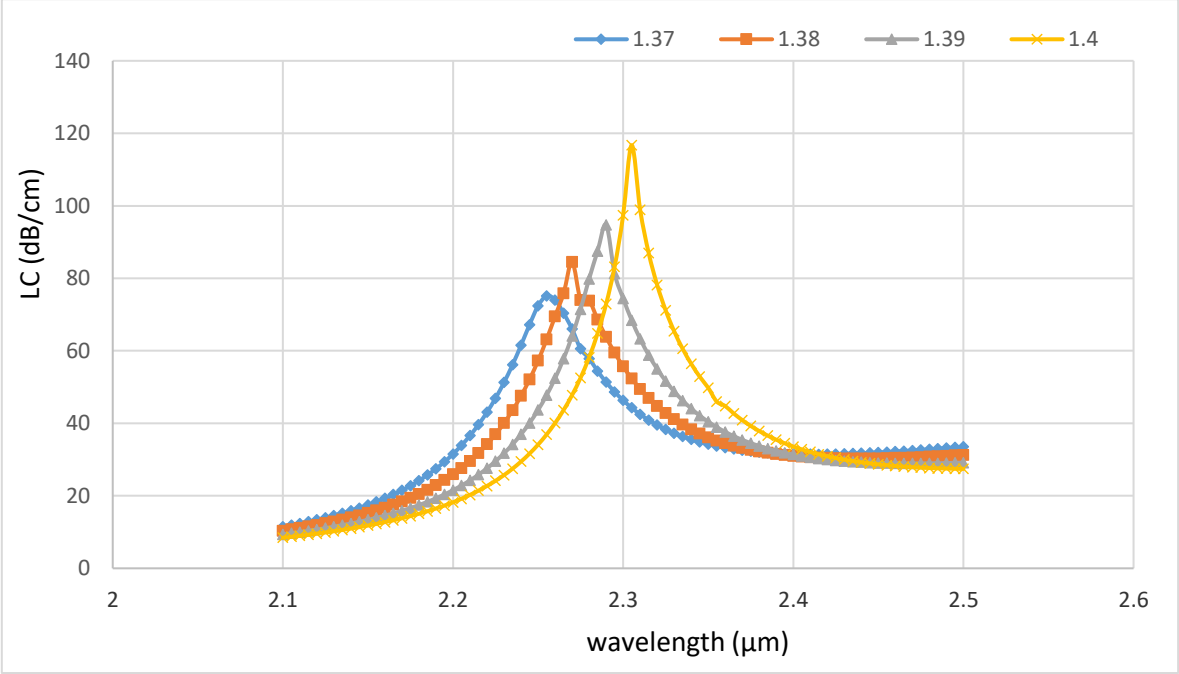

b

Figure (7): represents the confinement loss for nickel metal with the wavelength when ($n_a = 1.37,\ 1.38,\ 1.39,\ 1.40$), Where (a) represents ($R_2 = 1.8\ \mu m$) and (b) represents ($R_2 = 1.9\ \mu m$).

Figure (8) represents the relationship between the resonance wavelength with the ($n_a = 1.37,\ 1.38,\ 1.39,\ 1.40$) when ($R_2 = 1.8,\ 1.9\ \mu m$). It can be seen from the figure that the

relationships are almost linear, but they can be accepted to achieve ideal sensor conditions, and the best case is ($R_2 = 1.9\ \mu m$).

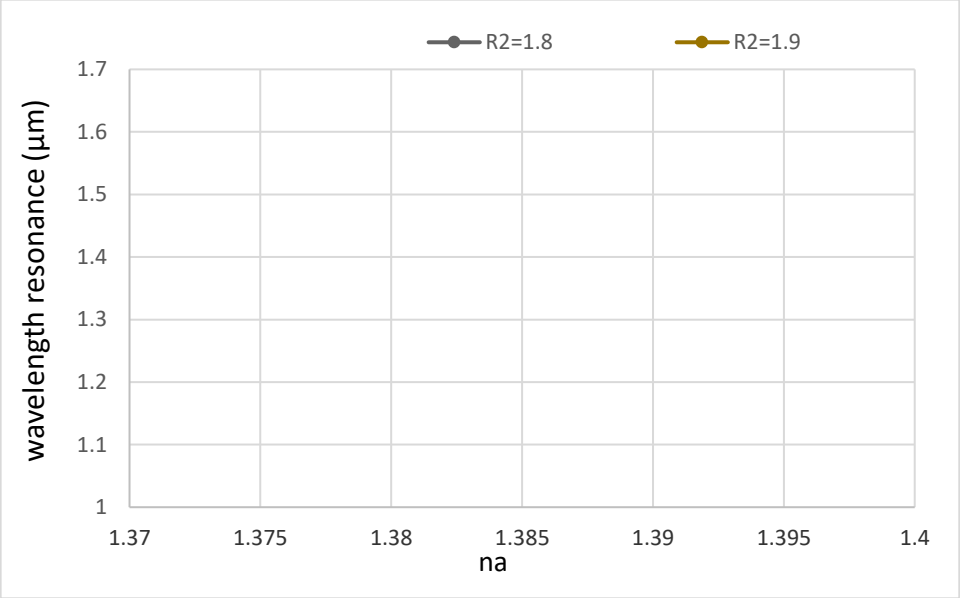

Figure (8): represent the resonance wavelength is represented with the ($n_a = 1.37,\ 1.38,\ 1.39,\ 1.40$) when ($R_2 = 1.8,\ 1.9\ nm$).

4.4 Effects of Core Radius (r1)

Figure (9): represents the relationship between the Lc λ of the ($n_a = 1.37,\ 1.38,\ 1.39,\ 1.40$) and the radius of the core ($r_1 = 2.3,\ 2.4\ \mu m$). From the figure, we notice that the highest peak appears in case ($r_1 = 2.4\ \mu m$), which is when ($n_a = 1.37$), then the peaks begin to decrease with the increase in the values of (n_a), and this case is similar to the case when ($r_1 = 2.3\ \mu m$). Table (3) summarizes the wavelength sensitivity achieved at different distances (r_1).

Table (6): Wavelength sensitivity at different distances r_1 .

$r_1(\mu m)$	Wavelength sensitivity (nm/RIU)
2.3	2500, 1500, 2000
2.4	3000, 2000, 2500

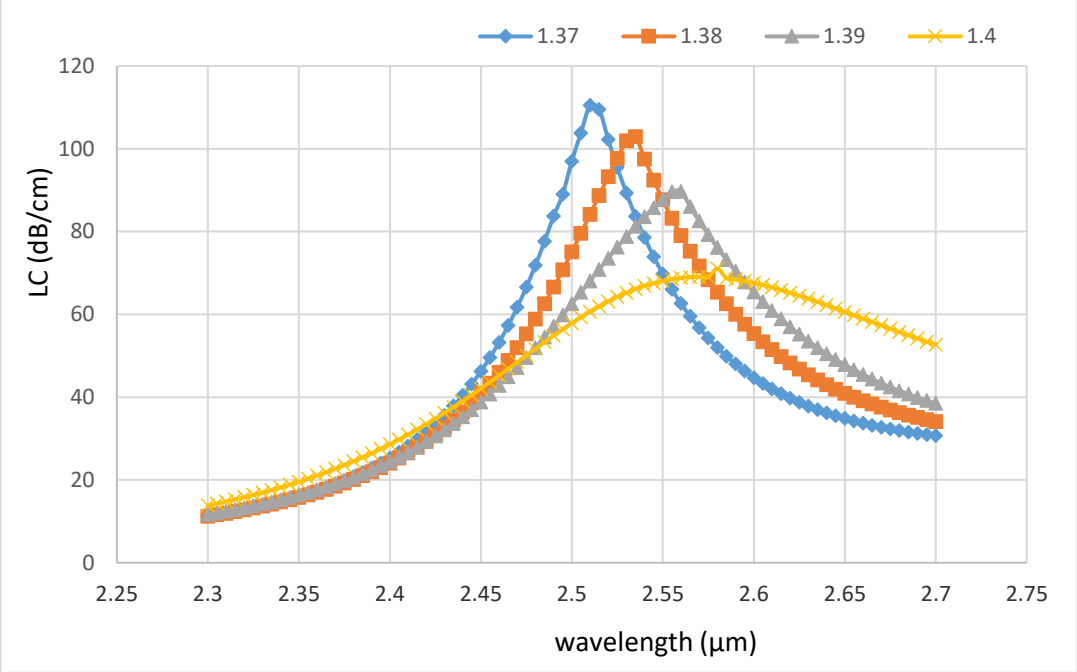

a

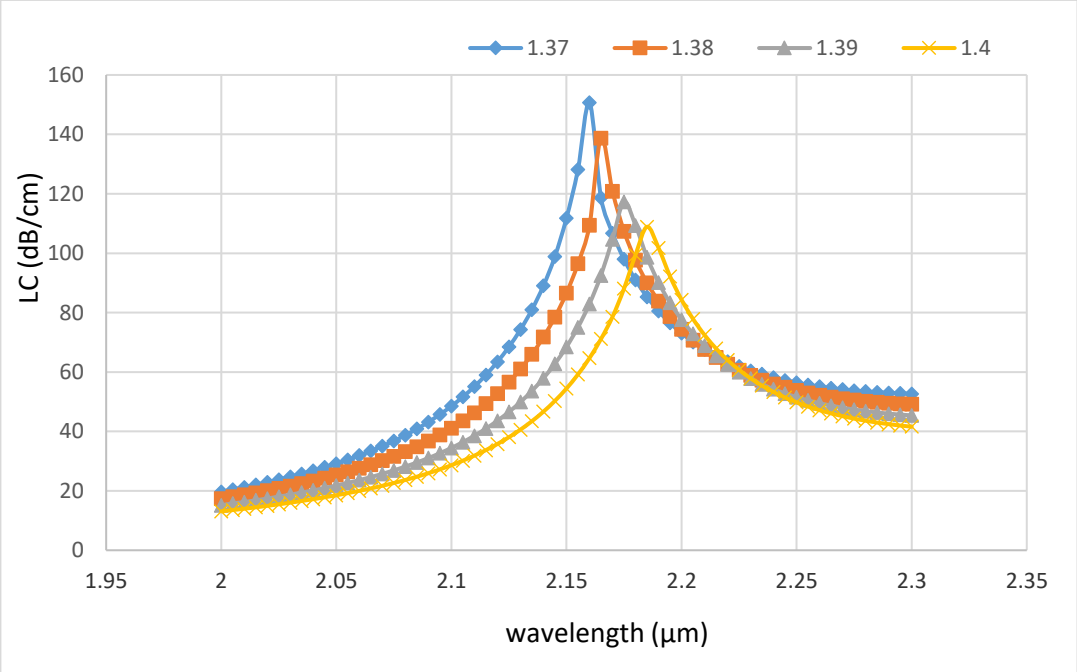

b

Figure (9): represents the confinement loss for nickel metal with the wavelength when ($n_a = 1.37,\ 1.38,\ 1.39,\ 1.40$), Where (a) represents ($r_1 = 2.3\ \mu m$) and (b) represents ($r_1 = 2.4\ \mu m$).

Figure (10) shows the resonance wavelength with the, n_a using the radii of the cores ($r_1 = 2.3,\ 2.4\ \mu m$). The relationships are approximately linear for all values of (r_1), but the best case is achieved when ($r_1 = 2.3\ \mu m$) and then ($r_1 = 2.4\ \mu m$).

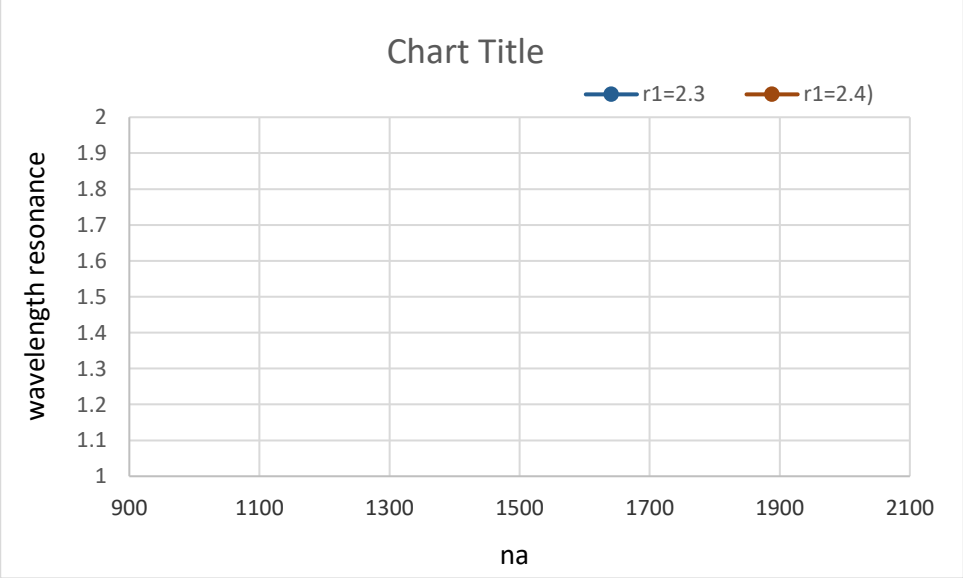

Figure 10: Resonance wavelength with the ($n_a = 1.37,\ 1.38,\ 1.39,\ 1.40$) when ($r_1 = 2.3,\ 2.4\ nm$).

4.5 Effects of the distance of Analyte Holes from Center (h)

Figure (11) shows the Lc with of the wavelength of different ($n_a = 1.37,\ 1.38,\ 1.39,\ 1.40$) using the analyte gap distance ($h = 9,\ 9.5\ \mu m$). It is observed from the figure that the highest value appears in the case of ($h = 9\ \mu m$) when ($n_a = 1.37$) and then begins to decrease with an increase (n_a), and this is the opposite case to case ($h = 9.5\ \mu m$). Table (7) summarizes the wavelength sensitivity achieved at different distances (h).

Table (7): Wavelength sensitivity at different distances h.

$h(\mu m)$	Wavelength sensitivity (nm/RIU)
9	1000, 1000, 1500
9.5	2500, 3000, 3000

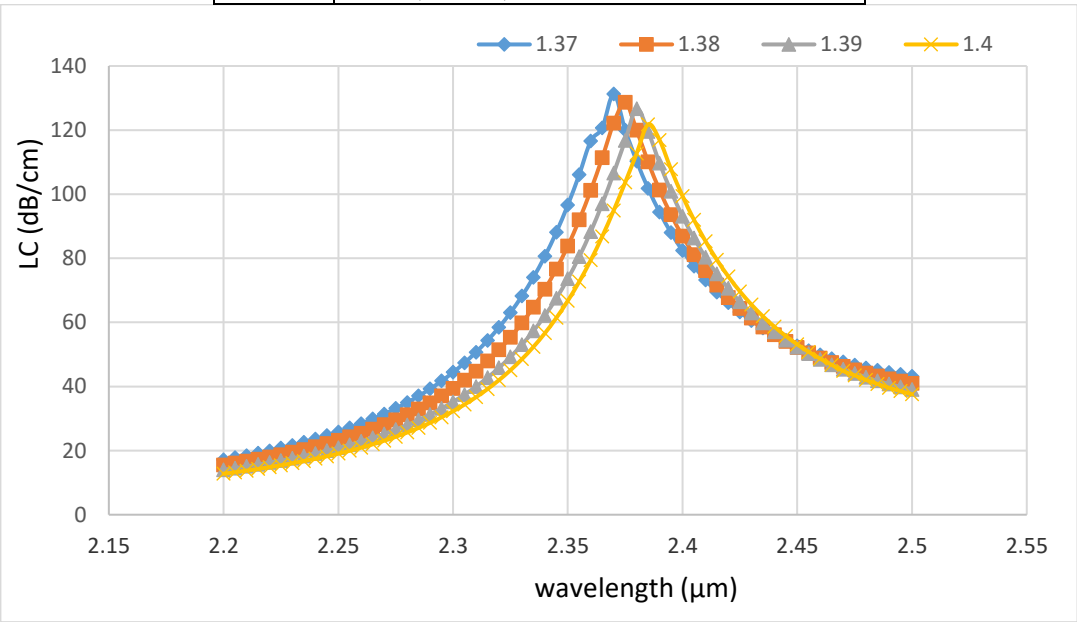

a

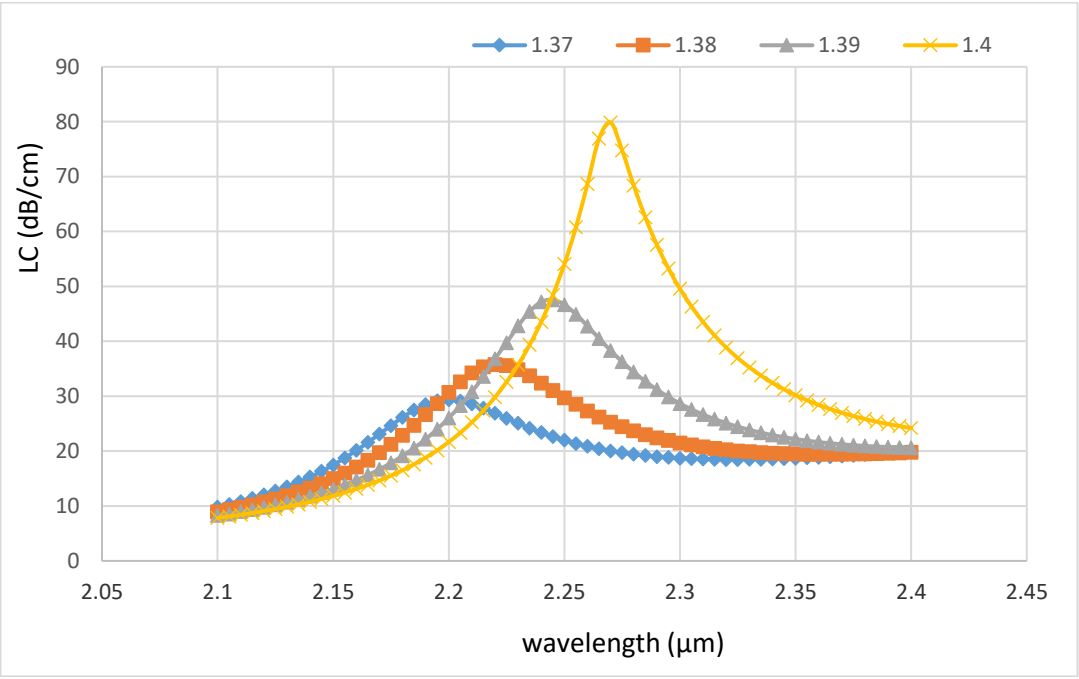

b

Figure (11): represents the confinement loss of nickel metal as a function of wavelength when ($n_a = 1.37,\ 1.38, 1.39, 1.40$), Where (a) represents ($h = 9\ \mu m$) and (b) represents ($h = 9.5\ \mu m$).

Figure (12) represents the resonance wavelength n_a at the hole distance ($h = 9,\ 9.5\ \mu m$). It is observed from the figure that in all cases of (h), the relationship is mostly linear, as we note that the best linear case is ($h = 9\ \mu m$) and then ($h = 9.5\ \mu m$).

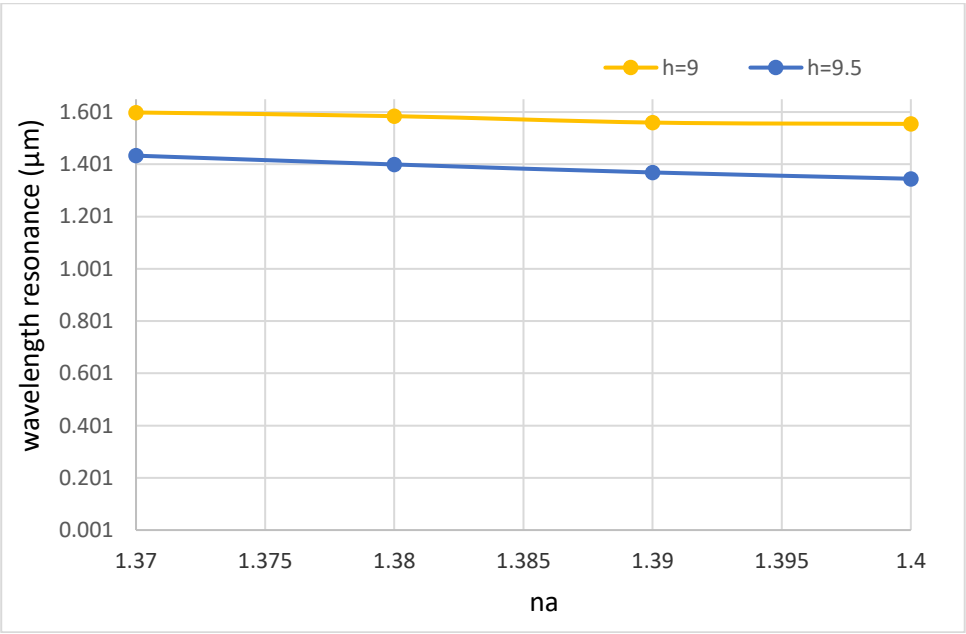

Figure (12): The resonance wavelength with the ($n_a = 1.37,\ 1.38, 1.39, 1.40$) when ($r_1 = 9,\ 9.5\ \mu m$).

5. Conclusions

The proposed high-sensitivity SPR-based PCF sensor is described and analyzed. The results showed that the first peaks of all the values of the parameter (h) shown in the

figures were when ($n_a = 1.4$) because it is closer to the refractive index of silica. It was also observed that the wavelength sensitivity increases significantly with decreasing h values. The capacitance sensitivity and the confinement loss are also affected by the value of (n_a), especially when it is slightly off the refractive index of silica. The designed sensor always has good linearity and all-state performance.

References

1. F. Zolla, G. Renversez, A. Nicolet, B. Kuhlmey, S. R. Guenneau, and D. Felbacq, Foundations of photonic crystal fibres: World Scientific, 2005.
2. D. Chen, M.-L. Vincent Tse, and H.-Y. Tam, "Super-lattice structure photonic crystal fiber," Progress in Electromagnetics Research, vol. 11, pp. 53-64, 2010.
3. S. B. Libori, J. Broeng, E. Knudsen, A. Bjarklev, and H. R. Simonsen, "High-birefringent photonic crystal fiber, "in OFC 2001. Optical Fiber Communication Conference and Exhibit. Technical Digest Postconference Edition (IEEE Cat. 01CH37171), pp. TuM2-TuM2, 2001.
4. R. Wang, J. Yao, Y. Miao, Y. Lu, D. Xu, N. Luan, et al., "A reflective photonic crystal fiber temperature sensor probe based on infiltration with liquid mixtures, "Sensors, vol. 13, pp. 7916-7925, 2013.
5. W. Wadsworth, J. Knight, W. Reeves, P. S. J. Russell, and J. Arriaga, "Yb/sup 3+/-doped photonic crystal fiber laser," Electronics Letters, vol. 36, pp. 1452-1454, 2000.
6. P. Jia, "Plasmonic Optical Sensors: Performance Analysis and Engineering Towards Biosensing," 2014.
7. X. Yang, Y. Lu, B. Liu, and J. Yao, "Analysis of graphene-based photonic crystal fiber sensor using birefringence and surface plasmon resonance," Plasmonics, vol. 12, pp. 489-496, 2017.
8. L. Wei, Advanced Fiber Sensing Technologies: Springer, 2020.
9. A. k. paul, A. k. sarkar, A. S. Rahman, and A. Khduleque., "Twin core photonic crystal fiber plasmonic refractive index sensor", IEEE sensors J., Vol. 18, No. 14, 2018.
10. R. K. Gangwar and V. K Singh, "Highly Sensitive Surface Plasmon Resonance Based D-Shaped Photonic Crystal Fiber Refractive Index Sensor", Plasmonics journal, Vol. 12, pp. 1367–1372, 2016.
11. S. Das and V. K. Singh, "Refractive Index Sensor Based on Selectively Liquid Infiltrated Birefringent Photonic Crystal Fiber", Optik journal, Vol. 201, 163489, 2020.
12. H. K. Muhammad, M. H. Salman, and H. A. Yasser, "New Plasmonic Photonic Crystal Fiber Sensor based on Core Size," NeuroQuantology, vol. 18, p. 45, 2020.
13. N. Kumar and B. Suthar, Advances in Photonic Crystals and Devices: CRC Press, 2019.
14. A. K. Paul, A. K. Sarkar, A. B. S. Rahman, and A. Khaleque, "Twin core photonic crystal fiber plasmonic refractive index sensor, "IEEE Sensors Journal, vol. 18, pp. 5761-5769, 2018.
15. A. K. Paul, M. S. Habib, N. H. Hai, and S. A. Razzak, "An air-core photonic crystal fiber based plasmonic sensor for high refractive index sensing," Optics Communications, vol. 464, p. 125556, 2020.
16. M. H. Salman, H K. Muhammad, H. A. Yasser, "Effects of holes radius on plasmonic photonic crystal fiber sensor with internal gold layer", Periodicals of Engineering and Natural Sciences , Vol. 8, No. 3, pp.1288-1296, 2020.
17. H K. Muhammad, M. H. Salman, H. A. Yasser, " New Plasmonic Photonic Crystal Fiber Sensor based on Core Size ", Neuro Quantology, Vol. 18, No. 9, pp. 45-53, 2020.
18. DNHD. J. J Hu, H. P. Ho, "Recent advances in plasmonic photonic crystal fibers: design, fabrication and applications", Advances in Optics and Photonics, Vol.9, No.2,2017.